Optik 125 (2014) 5268–5272

Contents lists available at ScienceDirect

Optik

journal homepage: www.elsevier.de/ijleo

# Optimal design for extending the lifetime of thin film luminescent solar concentrators

S.M. El-Bashir[a,b,*], O.A. AlHarbi[a], M.S. AlSalhi[a]

[a] Department of Physics & Astronomy, Science College, King Saud University, Riyadh, Saudi Arabia
[b] Department of Physics, Faculty of Science, Benha University, Egypt

ARTICLE INFO

*Article history:*
Received 21 August 2013
Accepted 15 May 2014

*Keywords:*
$PMMA/SiO_2$ nanohybrids
Coumarin dyes
Photostability

ABSTRACT

This study is concerned with the enhancement of the molecular, weathering stability of two models of thin film luminescent solar concentrators (LSCs). Two model systems of thin film LSCs had been proposed; the first model consists of a transparent $PMMA/SiO_2$ nanohybrid layer coated on a coumarin doped PMMA substrate. The second model designed as the ordinary configuration in which coumarin dye is dissolved in $PMMA/SiO_2$ nanohybrid layer then coated on a transparent PMMA substrate. The effect of nanosilica concentration on the prepared models was studied by TEM, SEM, DSC, FT-IR, UV–vis absorption and indoor photodegradation test. The obtained results suggested the first model for a durable design of thin film LSC applications specially in hot regions.



## 1. Introduction

Photovoltaics (PVs) enable the conversion of solar light into electricity without polluting the environment, the idea of solar energy concentration is considered a suitable way of decreasing the cost of photovoltaic energy conversion [1]. The standard methods of light concentration such as mirrors and lenses requires sun tracking, which only work for a narrow range of solar radiation and poorly suited to capture diffused solar radiation [2]. In the late 1970s the luminescent solar concentrator (LSC) had appeared as an alternative that it can avoid all of these disadvantages [3], and the technology was studied intensely through the early 1980s until the limitations of organic laser dyes hindered further development [4,5]. Fig. 1 shows a the operation principle of LSC device, it consists of a transparent plate where highly luminescent centers are embedded, a typical design consists of PMMA plate doped with a fluorescent material such as organic laser dye [6]. The dye molecules absorb a part of solar spectrum and the luminescent emission is guided by a light-pipe effect to the edge of LSC where the photovoltaic cells are attached. The main advantages of LSCs are; concentration of direct solar radiation without tracking the sun, high collection efficiency of diffused light, good heat dissipation from large areas of the LSC plate in contact with air, concentrated light could be optimized to match the spectral sensitivity of PV cells, besides the materials used in manufacturing LSCs are cost effective so the price of the PV cell is less important in the cost of the total system [7]. Materials used for manufacturing LSCs should have the properties tailored to meet the requirements set by the spectral distribution, intensity, and the angle of incidence the electromagnetic radiation [8]. The science and technology of such materials have soared during the past three decades as a result of the growing demand, cost, and environmental impact of energy production [9], $PMMA/SiO_2$ nanohybrid is considered a promising host matrix for organic luminescent dyes [10]. On the other hand the literature has a large number of papers published about luminescent plates in which the dye is incorporated in the entire bulk of the plate [11,12]. The LSC configuration in which the plate is covered by a thin film incorporating the colorant deposited in close contact with the plate had proved a better performance due to the decrease of parasitic losses resulting from self-absorption and scattering from impurities that usually found in bulk doped plates [13,14]. In the present study we employed two model systems of thin film LSCs depicted by Fig. 2. Model (1) consists of a transparent $PMMA/SiO_2$ nanohybrid layer coated on a fluorescent PMMA substrate. Model (2) in which the luminescent dye is dissolved in $PMMA/SiO_2$ nanohybrid layer then coated on a transparent PMMA substrate, this style is similar to that studied by Dienel et al. [14]. Our study aims to compare between the two models in order to choose the more stable one for outdoor application of thin film LSCs in hot countries.

* Corresponding author at: Department of Physics & Astronomy, Science College, King Saud University, Riyadh, Saudi Arabia.
*E-mail address:* elbashireg@yahoo.com (S.M. El-Bashir).

http://dx.doi.org/10.1016/j.ijleo.2014.06.046
0030-4026/

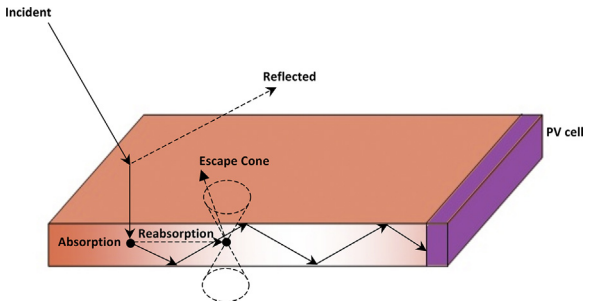


**Fig. 1.** The operation principle of luminescent solar concentrator (LSC).

## 2. Experimental technique

### 2.1. Preparation of LSC models

Before preparing the nanohybrid films the moisture adsorbed on the surface of hydrophilic nanosilica ($SiO_2$ Aldrich, S5130 powder, 7 nm) was removed by placing the nanosilica powder in an electric oven at $100 \pm 5\,^{\circ}C$ and weighting each hour until two consecutive weights are the same. After that PMMA (Aldrich, MW 350 k), hydrophilic nanosilica and red coumarin dyestuff (MACROLEX Fluorescent Red G, Bayer) were mixed separately in chloroform ($CHCl_3$). Transparent PMMA substrates were prepared by pouring PMMA/$CHCl_3$ solution in a rectangular glass mold; applying the same procedure fluorescent PMMA substrates were prepared by doping PMMA/$CHCl_3$ solution with 200 ppm coumarin dyestuff. After that the substrates were cut in dimensions $4\,cm \times 1\,cm \times 0.3\,cm$ and then coated with PMMA/$SiO_2$ nanohybrids. Two groups of LSC models were prepared; the first group consists of fluorescent PMMA substrates coated by transparent PMMA/$SiO_2$ nanohybrid with nanosilica concentrations ranging from 0.05 to 1 wt%. The second group consists of transparent PMMA substrates coated by fluorescent PMMA/$SiO_2$ nanohybrid with nanosilica concentrations ranging from 0.05 to 1 wt% and all doped with 200 ppm coumarin dyestuff. All the hybrid solutions were sonicated for 6 h before pouring on the as prepared substrates and spin coated in a centrifuge at 2000 rpm for 1 min to obtain uniform film coverage [15]; then they are left to dry in an electric oven at $40\,^{\circ}C$ for 6 h. The film thicknesses were measured using a profilometer (Talystep, Taylor Hobson, UK) on a scratch made immediately after deposition of five independent

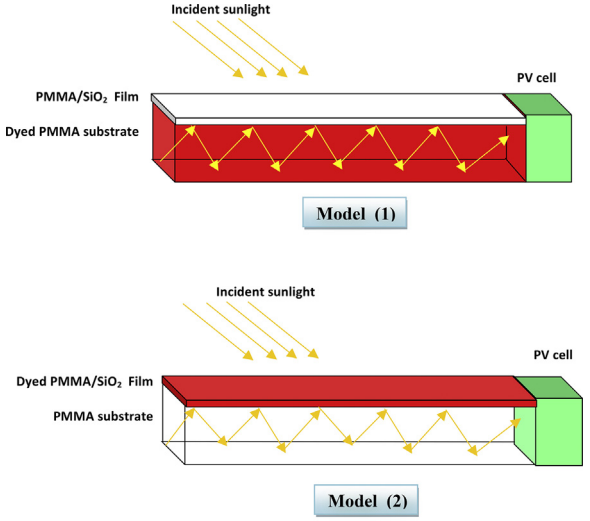


**Fig. 2.** The proposed thin film LSC models.

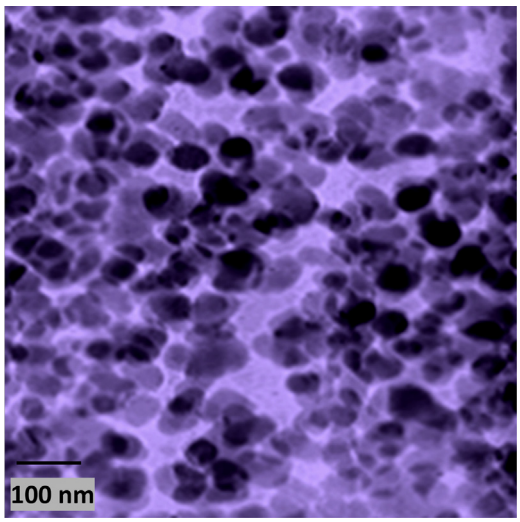


**Fig. 3.** TEM photograph of PMMA/$CHCl_3$/1 wt% $SiO_2$ nanohybrid solution before sonication.

measurements on each sample [16], and found to be in the range of $50 \pm 10\,\mu m$.

### 2.2. Measurements

TEM was performed by transmission electron microscope (JEOL JEM-1400, Japan). SEM characterization was performed by scanning electron microscope (JEOL, JSM-5400, Japan). FT-IR spectra were recorded by FT-IR spectrophotometer (Genesis Series, USA) in the wavenumber range ($4000–400\,cm^{-1}$). The differential scanning calorimetry (DSC) was carried out from room temperature to $150\,^{\circ}C$ in nitrogen atmosphere with a heating rate $20\,^{\circ}C$/min using equipment type (Setaram 131, France) for all the as prepared fluorescent PMMA/$SiO_2$ nanohybrids. The absorption spectra of the hybrid films were recorded in the wavelength range (200–900 nm) by a UV–VIS spectrophotometer (UNICAM, Helios Co., Germany). The photoresponse of the optimized nanohybrid films toward simulated sunlight was performed using a Xenon-arc lamp with the aid of the photodegradation accelerator (SUNTEST XLS+, Germany). The films were irradiated by $1200\,kJ\,m^{-2}\,h^{-1}$ continuously for 24 h to eliminate the dark reactions which might occur under normal day–night cycles. This period is equivalent to the global solar irradiance for about one year exposure to natural sunlight and the apparatus was regulated to match the climatic conditions of Riyadh city, the capital of Saudi Arabia.

## 3. Results and discussion

### 3.1. TEM and SEM characterization of PMMA/$SiO_2$ nanohybrid solution

Fig. 3 shows TEM photograph of PMMA/$CHCl_3$/1 wt% $SiO_2$ nanohybrid polymer solution before sonication. It is clear that all $SiO_2$ nanoparticles have a spherical shape of about 25 nm and fused to each other with a large tendency to form aggregates in the polymer solution. This was confirmed by SEM micrograph showed in Fig. 4a, it is clear that $SiO_2$ nanoparticles are aggregated into non-uniform shapes with average diameter size ranging from 140 to 250 nm. After sonication of the nanohybrid polymer solution for 6 h, it is observed that the size of these aggregates is reduced to about fifth of its value as determined from Fig. 4b. This convinced that the sonication process is important to reduce the probability

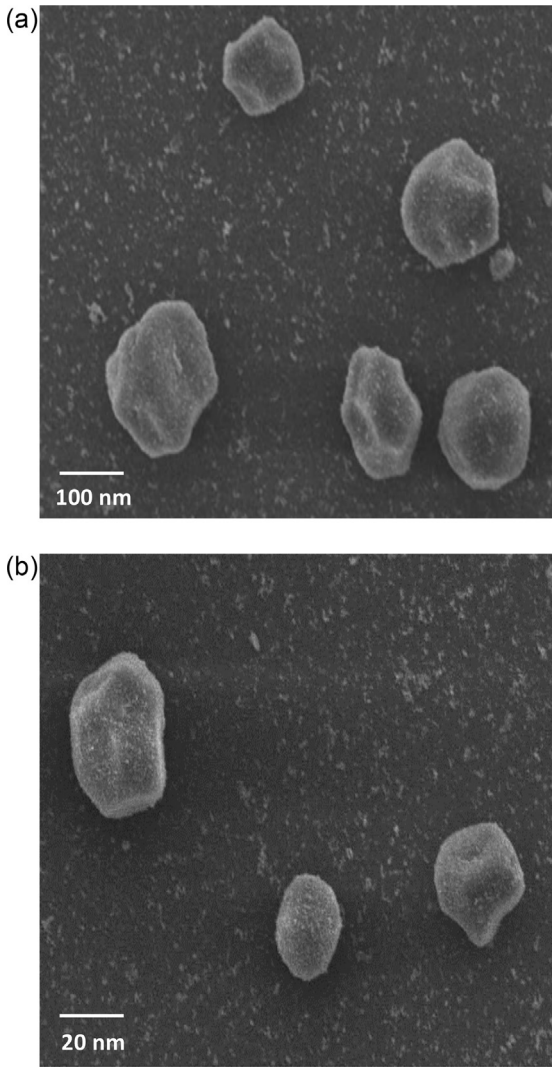


**Fig. 4.** SEM photograph of PMMA/$CHCl_3$/1 wt% $SiO_2$ nanohybrid solution (a) before sonication and (b) after sonication for 6 h.

of the formation of $SiO_2$ aggregates caused by hydrogen bonding between silanol groups (Si—OH) and hydroxyl groups (—OH) that exist on nanosilica surfaces during the manufacturing process [17].

### 3.2. DSC measurements of PMMA/$SiO_2$ nanohybrid coatings

DSC is an efficient tool used to monitor important parameters when working with polymers, it is widely used to characterize the thermophysical properties which is directly related to the homogeneity and stability of polymer nanohybrids. The effect of nanosilica concentration on the glass transition temperature $T_g$ of PMMA/$SiO_2$ nanohybrid films is clarified by DSC thermograms shown in Fig. 5, it is clear that the entire thermograms exhibit one glass transition, reflecting the homogeneity of the prepared nanohybrid films [18]. It is also observed that, the value of $T_g$ is shifted to higher temperatures from 110 °C for PMMA to 130 °C for PMMA/1 wt% $SiO_2$ nanohybrid film. This study confirms the enhancement of the thermal stability for PMMA/$SiO_2$ nanohybrid films by increasing nanosilica concentration and suggests their outdoor resistance toward hot climates in Saudi Arabia.

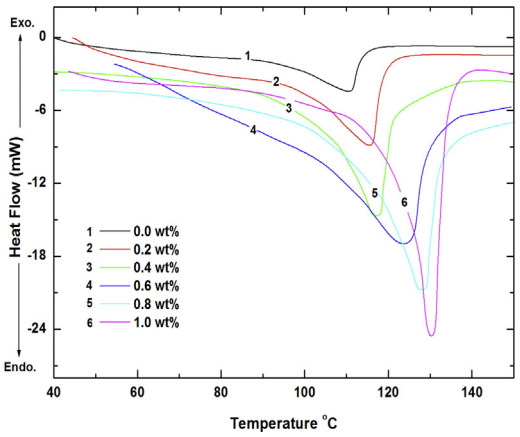


**Fig. 5.** The effect of nanosilica concentration on the glass transition temperature $T_g$ of PMMA/$SiO_2$ nanohybrids.

### 3.3. FT-IR characterization of PMMA/$SiO_2$ nanohybrid coatings

The effect of nanosilica concentration on the interactions between the vibrational energy states of fluorescent PMMA/$SiO_2$ nanohybrids films was investigated by FT-IR spectroscopic technique. Fig. 6 shows the FT-IR transmission spectra of PMMA/$SiO_2$ nanohybrid films in the selected wavenumber ranges (3700–3600 $cm^{-1}$) and (1800–1600 $cm^{-1}$). In the first range, it is noted that the weak shoulder appeared around (3650 $cm^{-1}$) in PMMA became well separated to a slightly asymmetric sharp peak shifted toward lower frequencies due to the emergence of fundamental stretching vibration of Si—OH groups by increasing nanosilica concentration [19,20]. The appearance of three bands in the range (3660–3600 $cm^{-1}$) indicates that the —OH groups have three different environments [21], which is a clear evidence of their interaction with three different molecules: PMMA through carbonyl group (C=O); coumarin molecule; and other (—OH) groups [2]. The second FT-IR range showed significant changes in the strong band corresponding to symmetric stretching mode of carbonyl group C=O of PMMA appeared at 1728 $cm^{-1}$ [22]. After adding $SiO_2$ nanoparticles, it is clearly observed that the band width

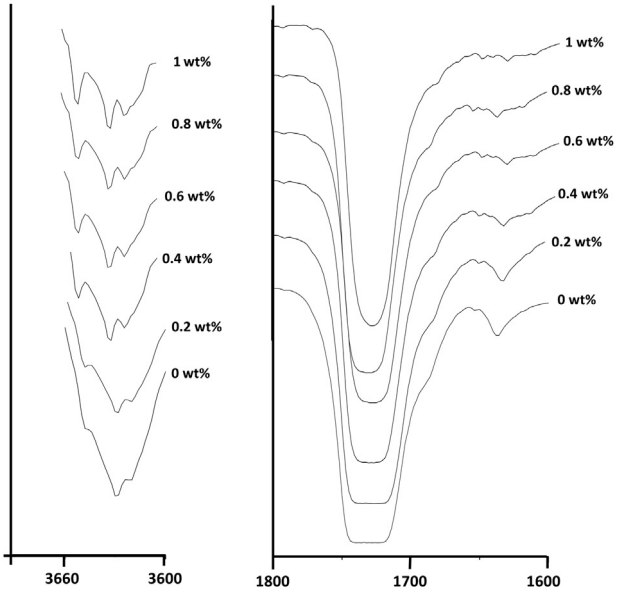


**Fig. 6.** Expanded FT-IR spectra in the ranges (3700–3600 $cm^{-1}$) and (1800–1600 $cm^{-1}$) for fluorescent PMMA/$SiO_2$ nanohybrids at different nanosilica concentrations.

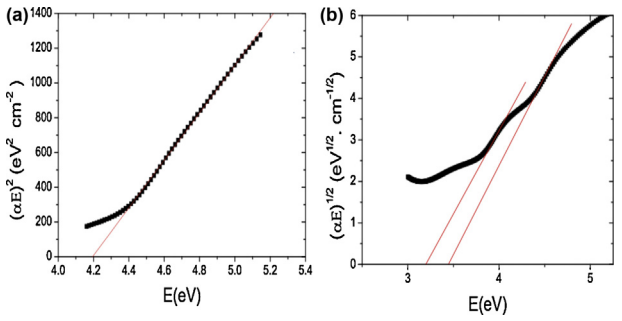


**Fig. 7.** Interband transitions for model (1) LSC sample at 0.7 wt% nanosilica concentration (a) direct and (b) indirect transition.

(FWHM) of C=O group is reduced from 50 to 40 $cm^{-1}$ accompanied with the disappearance of shoulder appeared at 1680 $cm^{-1}$ in PMMA. These changes reflect the strong interaction of C=O with surface hydroxyl group of hydrophilic nanosilica thus supports the enhanced chemical stability of thin-film LSCs based on PMMA/$SiO_2$ nanohybrid films.

### 3.4. HOMO–LUMO interband transitions in LSC models

Interband transitions of the prepared LSC models were analyzed in order to identify the electronic transitions from the highest occupied molecular orbital(s) (HOMO) of the valence band to the lowest unoccupied molecular orbital(s) of the conduction band (LUMO) which are directly related to the matrix stability [23,24]. The absorption coefficient "$\alpha$" of photon energy "$E$" is related to the type of the band transition and the band gap can be calculated by plotting a graph between $(\alpha E)^{1/m}$ versus "E" looking for the value of "$m$" depending on the nature of transition [24–26]. The allowed direct and indirect interband transitions are given by the values of "$m$" as 1/2 and 2, respectively, using equations:

$$(\alpha E)^2 = A(E - E_{gd})^{1/2} \quad (1)$$

$$\alpha E = B\left[\frac{(E - E_{gi} + E_p)^2}{\exp(E_p/kT) - 1} + \frac{(E - E_{gi} - E_p)^2}{1 - \exp(-E_p/kT)}\right] \quad (2)$$

where $A$ and $B$ are constants, $k$ is Boltzmann constant, $T$ is the absolute temperature, $E_p$ is the phonon energy, $E_{gd}$ and $E_{gi}$ are the energies of direct and indirect interband transitions respectively. According to Eqs. (1) and (2), there will be a single straight line for direct transitions and two linear portions for indirect transitions. Eqs. (1) and (2) were applied for all the LSC models and the relation between $(\alpha E)^2$ against "$E$" is plotted in Fig. 7a which is a representative diagram for all the LSC models. It noticed that all the samples have the same behavior in their direct allowed transitions for the two LSC models, the values of direct interband transition, $E_{gd}$, were estimated from the intercept on the energy axis of the linear fit of and listed in Table 1.

On the other hand for model (1) samples, Fig. 7b shows that plotting $(\alpha E)^{1/2}$ against "$E$" resolved into two distinct straight-line portions, the straight line was obtained at lower photon energies, cuts the energy axis at $E_{gi} - E_p$. The other line represents the dependence in the high energy range corresponding to a phonon-emission process and cuts the energy axis at $E_{gi} + E_p$, from the energy intercept of the two straight line portions, the values of the indirect HOMO–LUMO transition $E_{gi}$ could be estimated and listed in Table 1. It is noted that the values of $E_{gd}$ for model (1) samples are noticeably larger than those for model (2) samples this means that doping the dye in PMMA matrix introduced localized energy levels that form a continuum which act as trapping states and consequently increase $E_{gd}$. In contrast to the steadiness observed in the $E_{gd}$ values for model (2) samples, it is noted that model (1) exhibits some peculiar changes in the values of $E_{gd}$, in addition to the appearance of indirect interband transition $E_{gi}$ which can be attributed to the existence of different types of exciton like states [27]. This indicates the advantage of model (2) in reducing the probability of the dye interaction with matrix defects and consequently the stability of the photophysical processes through the HOMO–LUMO interband transitions [28].

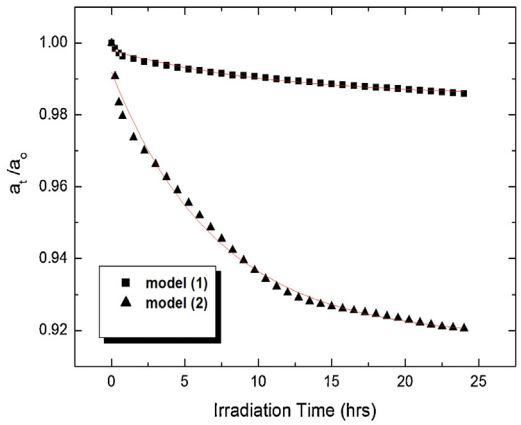


**Fig. 8.** The photodegradation curves of the LSC models having 1 wt% nanosilica concentration, after indoor exposure to artificial sunlight from Xenon arc lamp for 24 h.

### 3.5. Indoor photostability test

The long-term photostability of organic dyes is one of the most critical problems in LSC applications, the accelerated photoresponse of the investigated LSC models toward UV–vis radiation was investigated with the aid of artificial sunlight calibrated to match the typical solar spectrum on the Earth's atmosphere at AM1.5. The photodegradation "$a_t/a_o$", which is the hourly percentage change of the optical density after light irradiation is plotted against the exposure time as shown in Fig. 8. It is clear that the photodegradation of the dye molecules obeys 1st order exponential decay based on the following relation [10],

$$\frac{a_t}{a_o} = C_1 \exp(-Rt) + C_2 \quad (3)$$

where $a_t$ and $a_o$ are the absorbance values before and after irradiation for a period "$t$". $C_1$ and $C_2$ are the fitting constants and $R$ is the photodegradation rate constant of the dye molecules. This trend suggests two degradation mechanisms; the first concerns the dye

**Table 1**
The direct and indirect HOMO–LUMO interband transition energies for all the prepared LSCs models.

| Nano $SiO_2$ (wt%) | Model (1) LSCs | | Model (2) LSCs |
|---|---|---|---|
| | $E_{gd}$ (eV) | $E_{gi}$ (eV) | $E_{gd}$ (eV) |
| 0 | 4.20 | 3.46 | 3.59 |
| 0.05 | 4.30 | 3. 41 | 3.53 |
| 0.1 | 4.26 | 3.61 | 3.54 |
| 0.2 | 4.12 | 3.45 | 3.58 |
| 0.3 | 4.22 | 3.42 | 3.55 |
| 0.4 | 4.18 | 3.34 | 3.55 |
| 0.5 | 4.28 | 3.58 | 3.55 |
| 0.6 | 4.25 | 3.59 | 3.55 |
| 0.7 | 4.19 | 3.45 | 3.55 |
| 0.8 | 4.29 | 3.46 | 3.56 |
| 0.9 | 4.28 | 3.21 | 3.55 |
| 1 | 4.33 | 3.36 | 3.54 |

**Table 2**
Effect of nanosilica concentration on the degradation parameters "$R$" and $C_2$ of model (1) and model (2) LSCs.

| Nano $SiO_2$ (wt%) | Model (1) LSCs | | Model (2) LSCs | |
|---|---|---|---|---|
| | $R$ ($10^{-5}$ $s^{-1}$) | $C_2$ (%) | $R$ ($10^{-5}$ $s^{-1}$) | $C_2$ (%) |
| 0 | 17.2 | 85.3 | 42.8 | 80.4 |
| 0.05 | 11.3 | 86.4 | 40.4 | 81.0 |
| 0.1 | 9.2 | 87.6 | 37.6 | 82.4 |
| 0.2 | 8.7 | 88.7 | 31.1 | 83.2 |
| 0.3 | 8.2 | 89.3 | 27.2 | 84.3 |
| 0.4 | 7.3 | 90.4 | 23.1 | 85.6 |
| 0.5 | 6.2 | 91.7 | 20.6 | 86.4 |
| 0.6 | 5.8 | 93.6 | 17.5 | 87.3 |
| 0.7 | 5.1 | 95.4 | 11.6 | 88.7 |
| 0.8 | 4.9 | 96.8 | 9.4 | 89.3 |
| 0.9 | 4.1 | 97.4 | 6.9 | 90.8 |
| 1 | 2.5 | 99.0 | 3.9 | 92.0 |

molecules which may exist outside the free volume core between polymeric chains, and take a short time to photo-decompose at a rate constant "$R$". The second mechanism concerns the caged dye molecules inside PMMA–$SiO_2$ core and initiated after 2 h of irradiation, this period is approximately equal to 1 month of exposure to natural sunlight under normal atmospheric conditions. The values of "$R$" and $C_2$ were determined by least square fitting of Eq. (3) as depicted in Fig. 8, and listed in Table 2. It is clearly observed that, the value "$R$" is decreased by increasing nanosilica concentration for the two models. In addition, the absorbance of the residual amount of dye represented by $C_2$ indicates that the dye absorbance is enhanced by increasing nanosilica concentration for the two proposed LSC models, respectively. This means that model (2) LSC exhibits long outdoor lifetime compared to that of model (1). It is proposed that, transparent PMMA–$SiO_2$ nanohybrid coating can be considered as an effective solution for blocking harmful UV radiation [29] for the dye molecules doped in model (1) LSCs. On the opposite; for the case of model (2) LSCs, the dye molecules are directly subjected directly to UV radiation which plays a dominant role on the dye degradation by causing a perturbation in the number of $\pi$ electrons in the dye molecules [30].

## 4. Conclusions

This paper represented a study on modification of the design of thin film LSCs in order to develop effective characteristics for environmentally stable thin film LSCs. This has been done by covering the dye doped PMMA plate by a transparent PMMA/$SiO_2$ nanohybrid coating. FT-IR spectra showed the enhancement of the molecular bonding between PMMA and $SiO_2$ nanoparticles by increasing nanosilica concentration, this reflects chemical stability of the prepared films. Moreover, DSC measurements revealed the increase of $T_g$ values by increasing nanosilica concentration promoting long-term thermal stability of nanohybrid film. The study of interband transitions revealed the existence of only direct band transition in model (2) LSCs due to the limitation of the dye interaction with matrix defects. The accelerated photodegradation test for the modified LSC design (model 1) suggested the enhancement of the photostability of the dye molecules compared to the behavior observed for the ordinary design (model 2). In view of the results presented above, it is concluded that PMMA/$SiO_2$ nanohybrid film can act as a protective coating which can prevent the thermal and photodegradation of luminophores in thin film LSCs. The results of this study recommended model (1) LSCs as an ubiquitous part of the built environment specially in the hot regions that have a high value of UV index.

## Acknowledgement

This research project was supported by a grant from the "Research Center of the Center for Female Scientific and Medical Colleges", Deanship of Scientific Research, King Saud University.

## References

[1] T. Saraidarov, V. Levchenko, A. Grabowska, P. Borowicz, R. Reisfeld, Non-self-absorbing materials for luminescent solar concentrators (LSC), Chem. Phys. Lett. 492 (2010) 60–62.
[2] M.S. De Cardona, M. Carracosa, F. Meseguer, F. Cusso, F. Jaque, Outdoor evaluation of luminescent solar concentrator prototypes, Appl. Opt. 24 (1985) 2028–2032.
[3] A. Goetzberger, W. Greubel, Solar energy conversion with fluorescent collectors, Appl. Phys. 14 (1977) 123–139.
[4] B.C. Rowan, L.R. Wilson, B.S. Richards, Advanced material concepts for luminescent solar concentrators, IEEE J. Select. Topics Quantum Electron. 14 (2008) 1312–1322.
[5] R. Reisfeld, Prospects of sol–gel technology towards luminescent materials, Opt. Mater. 16 (2001) 1–7.
[6] R. Koeppea, N.S. Sariciftci, Enhancing photon harvesting in organic solar cells with luminescent concentrators, Appl. Phys. Lett. 90 (2007) 181126.
[7] A.F. Mansour, M.G. El-Shaarawy, S.M. El-Bashir, M.K. El-Mansy, M. Hammam, A qualitative study and field performance for a fluorescent solar collector, Polym. Test. 21 (2002) 277–281.
[8] J. Bomm, et al., Fabrication and full characterization of state-of-the-art quantum dot luminescent solar concentrators, Sol. Energy Mater. Sol. Cells 95 (2011) 2087–2094.
[9] V. Sholin, J.D. Olson, S.A. Carter, Semiconducting polymers and quantum dots in luminescent solar concentrators for solar energy harvesting, J. Appl. Phys. 101 (2007) 123114.
[10] M.G. El-Shaarawy, S.M. El-Bashir, M. Hammam, M.K. El-Mansy, Bent fluorescent solar concentrators (BFSCs): spectroscopy, stability and outdoor performance, Curr. Appl. Phys. 7 (2007) 643–649.
[11] R. Reisfeld, C.K. Jorgensen, Luminescent solar concentrators for energy conversion, Struct. Bond. 49 (1982) 1–36.
[12] J.S. Batchelder, A.H. Zewail, T. Cole, Luminescent solar concentrators. 1: Theory of operation and techniques for performance evaluation, Appl. Opt. 18 (1979) 3090–3110.
[13] R. Reisfeld, D. Shamrskov, C. Jorgensen, Photostable solar concentrators based on fluorescent glass films, Sol. Energy Mater. Sol. Cells 33 (1994) 417–427.
[14] T. Dienel, C. Bauer, I. Dolamic, D. Brühwiler, Spectral-based analysis of thin film luminescent solar concentrators, Sol. Energy 84 (2010) 1366–1369.
[15] E. Mohajerani, F. Farajollahi, R. Mahzoon, S. Baghery, Morphological and thickness analysis for PMMA spin coated films, J. Optoelectron. Adv. Mater. 9 (2007) 3901–3906.
[16] A. Pepe, P. Galliano, M. Aparicio, A. Duran, S. Cere, Sol–gel coatings on carbon steel: electrochemical evaluation, Surf. Coat. Technol. 200 (2006) 3486–3491.
[17] Fumed Silica Technical Bulletin, http://www.Sigma-Aldrich.com
[18] H.M. Zidan, A. Tawansi, M. Abu-Elnader, Miscibility, optical and dielectric properties of UV-irradiated poly(vinylacetate)/poly(methylmethacrylate) blends, Physica B 339 (2003) 78–86.
[19] H.L. Yeager, J.D. Fedyk, R.J. Parker, Spectroscopic studies of ionic solvation in propylene carbonate, J. Phys. Chem. 77 (1973) 2407–2410.
[20] S.A. Agnihotry, S. Ahmad, D. Gupta, S. Ahmad, Composite gel electrolytes based on poly(methylmethacrylate) and hydrophilic fumed silica, Electrochim. Acta 49 (2004) 2343–2349.
[21] M.L. Hair, Infrared Spectroscopy in Surface Chemistry, Marcel Dekker, Inc., New York, 1967.
[22] S.M. El-Bashir, A. Hendi, A decorative construction material prepared by making use of marble waste granules and PMMA/$SiO_2$ nanocomposites, Polym. Plast. Technol. Eng. 49 (2010) 78–82.
[23] R.M. Ahmed, S.M. El-Bashir, Structure and physical properties of polymer composite films doped with fullerene nanoparticles, Int. J. Photoenergy (2011) (Article ID 801409).
[24] A.F. Mansour, M.G. El-Shaarawy, S.M. El-Bashir, M.K. El-Mansy, M. Hammam, Optical study of perylene dye doped poly(methylmethacrylate) as fluorescent solar collector, Polym. Int. 51 (2002) 393–397.
[25] J.I. Pankove, Optical Processes in Semiconductors, Prentice Hall, Upper Saddle River, NJ, 1972.
[26] S. Saq'an, Y. Ramadin, M. Ahmad, A. Zihlif, F. Pavlovska, A. Trajkovska, Optical and dielectric properties of polyvinylchloride/polymethylmethacrylate blends, Polym. Test. 20 (2001) 919–923.
[27] B. Kulyk, V. Kapustianyk, V. Tsybulskyy, O. Krupka, B. Sahraoui, Optical properties of ZnO/PMMA nanocomposite films, J. Alloys Compd. 502 (2010) 24–27.
[28] M.D. Migahed, H.M. Zidan, Influence of UV-irradiation on the structure and optical properties of polycarbonate films, Curr. Appl. Phys. 6 (2006) 91–96.
[29] Y.H. Zhang, J.H. Xin, W.A. Daoud, X.Y. Hao, UV-blocking properties of silica/titania hybrid nanocomposites, Key Eng. Mater. 334–335 (2007) 1065–1068.
[30] A.N. Fletcher, Laser dye stability. Part 4, Appl. Phys. 16 (1978) 93–97.